Microfluidic microsphere-trap arrays for simultaneous detection of multiple targets

Xiaoxiao Xu, Zhenyu Li, Nalinikanth Kotagiri, Pinaki Sarder, Samuel Achilefu, et al.

Xiaoxiao Xu, Zhenyu Li, Nalinikanth Kotagiri, Pinaki Sarder, Samuel Achilefu, Arye Nehorai, "Microfluidic microsphere-trap arrays for simultaneous detection of multiple targets," Proc. SPIE 8615, Microfluidics, BioMEMS, and Medical Microsystems XI, 86151E (13 March 2013); doi: 10.1117/12.2006628

SPIE.

Event: SPIE MOEMS-MEMS, 2013, San Francisco, California, United States

Microfluidic Microsphere-Trap Arrays for Simultaneous Detection of Multiple Targets

Xiaoxiao Xu[a], Zhenyu Li[b], Nalinikanth Kotagiri[c], Pinaki Sarder[c], Samuel Achilefu[c], Arye Nehorai[*a]
[a]Preston M. Green Department of Electrical and Systems Engineering, Washington University in St. Louis, St. Louis, MO 63130, USA;
[b]Department of Electrical and Computer Engineering, The George Washington University, Washington, D.C., 20052, USA;
[c]The Mallinckrodt Institute of Radiology, Washington University School of Medicine in St. Louis, St. Louis, MO 63110, USA.

ABSTRACT

Microsphere arrays can be used to effectively detect, identify, and quantify biological targets, such as mRNAs, proteins, antibodies, and cells. In this work, we design a microfluidic microsphere-trap array device that enables simultaneous, efficient, and accurate screening of multiple targets on a single platform. Different types of targets are captured on the surfaces of microspheres of different sizes. By optimizing the geometric parameters of the traps, the trap arrays in this device can immobilize microspheres of different sizes at different regions with microfluidic hydrodynamic trapping. The targets are thus detected according to the microspheres' positions (position-encoding), which simplifies screening and avoids errors in target identification. We validate the design using fluid dynamics finite element simulations by COMSOL Multiphysics software using microsphere of two different sizes. We also performed preliminary microsphere-trapping experiments on a fabricated device using microspheres of one size. Our results demonstrate that the proposed device can achieve the position-encoding of the microspheres with few fluidic errors. This device is promising for simultaneous detection of multiple targets and become a cheap and fast disease diagnostic tool.

Keywords: Microfluidics, Microsphere-Trap Arrays, Simultaneous Detection of Multiple Targets

1. INTRODUCTION

1.1 Integrated microfluidic microsphere array system

Microsphere arrays are a powerful tool to detect and quantify biological targets, such as DNA, RNA, and proteins, which are key biomolecules for maintaining normal physiological and molecular activities in cells and organs. In the microsphere arrays, the microspheres are embedded with receptors on their surface that are specific for certain targets.[1-4] Therefore, these arrays have great potentials, such as the independent, quantitative, and simultaneous assay of multiple types of targets in small volumes of material, and collection of statistically rigorous data from numerous microspheres for each type of targets. Microfluidics technology provides the ability to analyze small volumes of sample, minimize costly reagent consumption, and reduce sample processing time. The integration of microfluidics technology with the microsphere arrays has a number of advantages, such as offering a gentle liquid environment for biological samples, reducing reagent cost and hybridization assay time, integrating high-throughput sample processing steps, and providing the potential for mass production of devices at low cost.[5,6] Therefore, the integrated microfluidic microsphere array system has played an increasingly important role in life science research and medical diagnostics.

1.2 Simultaneous detection of multiple targets

Advanced array systems are designed around detecting and correlating multiple analytes in solution. While suspension array technology (such as Luminex) sorts microspheres based on their colors,[4] a microfluidic microsphere array system has to achieve the same using position-encoding.[1] Specifically, for detecting multiple types of targets in the microfluidic system, conventional approaches are to use different labels (for example, fluorescent dyes at distinct emission wavelengths) to recognize different targets on the microspheres. However, in these approaches, the microspheres are

Further author information: (Send correspondence to A. Nehorai)
A. Nehorai: E-mail: nehorai@ese.wustl.edu, Telephone: 1 314 935 5565

Microfluidics, BioMEMS, and Medical Microsystems XI, edited by Holger Becker, Bonnie L. Gray, Proc. of SPIE
Vol. 8615, 86151E · © 2013 SPIE · CCC code: 0277-786X/13/$18 · doi: 10.1117/12.2006628

randomly placed so that the captured different targets are mixed. As a result, subsequent fluorescence imaging requires complex segmentation in data analysis, and the noise in the imaging makes the analysis even more prone to errors in identifying targets.[7-9] To solve the limitations of the label-based approaches, we have previously designed a microsphere array device with microspheres immobilized at predetermined locations (i.e., position-encoding) in a highly parallel and compact fashion.[1] Then target identification can be achieved according to the microspheres' positions, which simplifies screening and is error-free. For simultaneous detection of multiple targets, one possibility is to implement multiple channels connected with individual chambers on a microfluidic chip, and use on-chip valves to open or lock the channels to direct the microspheres for a specific type of targets to flow into a specific chamber.[10-15] While this approach can achieve multiplexing, a disadvantage is that the valves occupy a lot of space on the chip and most of the valves need a sophisticated actuation platform supplied by a control and actuation device.[16] Moreover, for effective collection of information such as profiling multiple proteins or simultaneous mRNA and protein profiling, there is a need and great interest for multianalyte detection in a single channel. Therefore, we aim to develop a simple, easy-controllable, efficient, and sensitive one-channel platform for simultaneous detection and quantification of multiple targets.

1.3 Our design

In our recent work, we designed a novel microfluidic microsphere-trap array device.[17] By microfluidic hydrodynamic trapping, the trap arrays immobilized microspheres with targets on their surfaces. We developed a comprehensive and robust framework to optimize the values of the trap arrays' geometric parameters to achieve the following goals: (1) maximize the microspheres' packing density, (2) efficiently immobilize a single microsphere in each trap, that is to eliminate fluidic errors such as channel clogging and multiple microspheres in a single trap, and (3) minimize errors in subsequent imaging experiments. Through microsphere-trapping experiments on the optimized device and an un-optimized device, we demonstrated the superior performance of our optimized device.

Our previous design and optimization framework aim to detect and quantify a single type of targets captured on the surfaces of microspheres of a single size. In this work, we design the trap arrays by proposing a simple but effective idea that extends our optimization framework for simultaneous, efficient, and accurate detection of multiple targets in a single-channel device. Specifically, we employ microspheres of difference sizes to capture different targets. We further optimize the geometric parameters of the traps, to separate and immobilize the different microspheres at different known regions in the same channel by hydrodynamic trapping, without using different channels (chambers) and on-chip valves. Finally, as stated, the targets are detected according to the microspheres' positions.[1] We validate the design through finite element fluid dynamics simulations for microspheres of two different sizes. We also perform preliminary microsphere-trapping experiments on a fabricated device using microspheres of one size. The results demonstrate that our device achieves the position-encoding of the microspheres with few fluidic errors. Therefore, this device for simultaneous detection of multiple targets in a single channel improves information gathering efficiency, reduces fabrication complexity, and is promising to become a fast and cheap disease diagnostic tool.

This paper is organized as follows. In Section 2, we describe the design strategy of the microsphere-trap arrays for simultaneous detection of multiple targets. As an example, we provide the optimized design of the trap geometry for detecting two types of targets. Section 3 shows the finite element fluidic dynamics simulation results of the two-type targets trap array design. Section 4 provides the preliminary results of the microsphere-trapping experiments using the fabricated device. Section 5 concludes the paper.

2. MICROFLUIDIC MICROSPHERE-TRAP ARRAYS FOR SIMULTANEOUS DETECTION OF MULTIPLE TARGETS

2.1 Design strategy

The design of the microfluidic microsphere array platform for simultaneous detection of multiple targets is based on our previous work, in which we proposed and implemented a microfluidic microsphere-trap array device to detect a single type of targets.[17] Here we briefly describe the general configuration of the device (chip), as shown in the schematic Fig. 1. The traps in the arrays are made of polydimethylsiloxane (PDMS). Each trap is made of inverted-trapezoid grooves. The platform has an inlet and an outlet to let through a fluidic stream, such as phosphate buffered saline (PBS). To fill the traps, the microfluid stream containing the microspheres with specific receptors flows through the channels. The microspheres are immobilized in the traps by hydrodynamic trapping mechanism during the flow process. In the arrays, each row of the traps is offset horizontally with respect to the one above it. This offset ensures the microspheres not trapped by the first row can easily be captured by the next row of traps.

In the previous design,[17] we developed an analytical method to optimize the values of the trap's geometric parameters to maximize the microsphere arrays' packing density to make the device compact. In this optimization, we simultaneously satisfied also other criteria, such as efficiently immobilizing a single microsphere in a single trap, effectively eliminating fluidic errors, achieving a feasible fabrication, and minimizing errors induced during the subsequent fluorescence imaging. Microsphere-trapping experiments performed using the optimized device demonstrate the easy-control of the transportation, immobilization, and manipulation of microspheres in the trap arrays. Further quantitative comparisons also show that the optimized device greatly outperforms the un-optimized device (the device with randomly selected values of the geometric parameters).

Here, for a simple and simultaneous screening of multiple types of targets on a single platform (chip), we propose to employ microspheres of difference sizes to detect different targets. We modify our design and optimization framework.[17] to select the geometric parameters of the traps, to immobilize the different-size microspheres at different known regions on a single chip surface by hydrodynamic trapping. Particularly, from the inlet to the outlet in the chip, the arrays of the largest traps are located nearest to the inlet, the upper and bottom openings of which are optimized to trap the largest microspheres and let through the other smaller microspheres. The arrays of the second largest traps followed subsequently after the largest trap arrays, which are designed to trap the second largest microspheres and let through the remaining smaller microspheres. Then the arrays of the third largest traps are located, so on and so forth. During the experiment, the fluidic stream containing microspheres of different sizes with different targets flows through the platform, and the different-sized microspheres are immobilized at their corresponding regions. Then the targets are identified by positions of their tagged microspheres (position-encoding).[1] The targets are further quantified by subsequent microscopy imaging. We note that ideally, the microspheres of different sizes should be loaded simultaneously to simply operation. Then to avoid overload of these microspheres, their concentrations should be carefully controlled so that the number of microspheres are less than the numbers of their corresponding traps. As a demonstration, in next subsection, we will present the design of the trap arrays for simultaneous detection of two types of targets, and the selection of their geometric parameters.

2.2 Microfluidic microsphere-trap arrays for simultaneous detection of two types of targets

To demonstrate the proposed design strategy, here we present the design for the microfluidic microsphere-trap arrays for simultaneous detection of two types of targets. In other words, we describe how we modify the optimization framework[17] to obtain the optimal geometric parameters of the trap arrays for immobilizing microspheres of two different sizes.

In Fig. 1, we show the schematic of the trap array geometries and depict the corresponding geometric parameters. In this schematic, microspheres of two distinct sizes (shown in blue and green colors) are encoded with two specific receptors (not shown here) to capture two types of targets. We term the microspheres with larger radius as the 'large' microspheres and denote their parameters with subscript '1'. Likewise, we term the other microspheres with smaller radius as the 'small' microspheres and denote their parameters with subscript '2'. The arrays of large traps for immobilizing the large microspheres are located at the front region in the chip, with the arrays of small traps for immobilizing the small microspheres follow after them in the back region. For the microsphere of the i^{th} $(i = 1, 2)$ size and its corresponding traps, we define the radius of the microsphere as r_i; the height of the trap groove as h_i; the length and the upper width of the groove walls as l_i and t_i, respectively; the trapezoid angle of the trap α_i; and the upper and the bottom widths of the trap opening as u_i and b_i, respectively. We also define the width of the channel in the microsphere's corresponding trap region as g_i, the distance between two microspheres in the same row as d_i, and the distance between a trap and a microsphere filled in a consecutive row as v_i. To eliminate the units of these parameters, we normalize them by dividing by the groove height h_i (see Fig. 1). We use below the sign ˜ to represent the resulting parameters; e.g., $\tilde{r}_i$ represents the normalized r_i. Furthermore, we define the area of a single large trap and its surroundings as S_i, and the packing density of the large trap arrays as ρ_i.

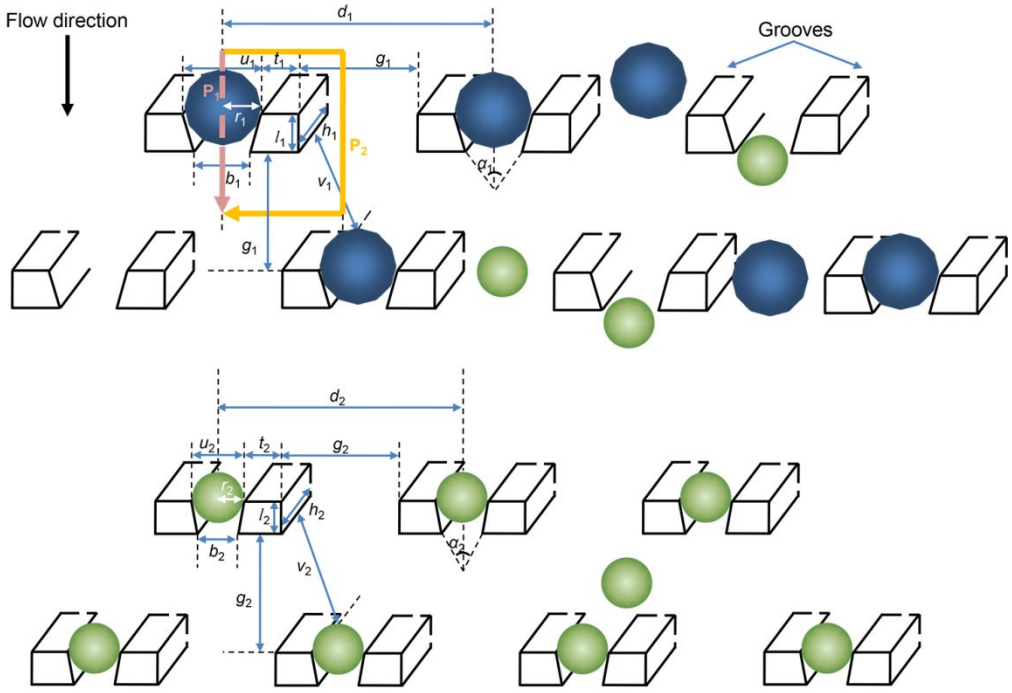

Fig. 1. Schematic diagram of microfluidic microsphere-trap array geometries for simultaneous detection of two types of targets. Microspheres of two distinct sizes (shown in blue and green colors) are encoded with two specific receptors (not shown here) to capture two types of targets. The corresponding trap arrays for immobilizing the microspheres are presented here, with two adjacent rows for microspheres of each size.

We first present our optimization framework[17] to obtain the optimal geometric parameters of the trap arrays for single-sized microspheres. The optimization objective to maximize the packing density $\rho_i, i = 1, 2$, which is equivalent to minimizing the area S_i with respect to the geometric parameters $\boldsymbol{\delta}_i = [r_i, h_i, l_i, u_i, b_i, t_i, g_i, d_i, v_i]^T$. The optimization problem is summarized as

$$\rho_{i,\text{opt}} = 1/S_{i,\text{opt}}, \text{ with } S_{i,\text{opt}} = h_i^2 \cdot \min_{\boldsymbol{\delta}_i}(\tilde{g}_i + \tilde{l}_i) \cdot (\tilde{u}_i + 2\tilde{t}_i + \tilde{g}_i), \quad (1)$$

where $\boldsymbol{\delta}_i \in \{C_1 \cap C_2 \cap C_3 \cap C_4 \cap C_5 \cap C_6\}$, with $C_j, j = 1, \ldots, 6$ as the optimization constraints. Here, we briefly review these constraints. More detailed descriptions and derivations are given in Ref. 17.

- Constraint C_1 is to ensure the desired hydrodynamic trapping. That is, the trap array geometry is designed so that path P_1 (pink line in Fig. 1) for an empty trap has a lower flow resistance than path P_2 (green line in Fig. 1). Then the microsphere in the fluid through the channels chooses path P_1 to move into an empty trap. However, once the trap through P_1 is filled by a microsphere, the flow resistance in P_1 increases and becomes larger than that in P_2. Thus, subsequent microspheres divert to path P_2 and bypass the filled trap. The specific representation of C_1 is given by Eqn. (7) in Ref. 17.
- Constraint C_2 is to ensure a single microsphere in each trap and avoid multiple microspheres trapped at one trap location. This constraint is given by constraining the upper width u_1 and bottom width b_i of the trap opening as well as the length of the groove walls l_i, i.e., $C_2 = \{\tilde{b}_i \le 2\tilde{r}_i - 2/h_i, \tilde{u}_i \le 4\tilde{r}_i - 2/h_i, \tilde{l}_i \le 4\tilde{r}_i - 2/h_i\}$.
- Constraint C_3 is to ensure stable trapping of the microspheres, i.e., a microsphere immobilized in a trap is retained in the trap and is not swept away due to the transient flow motion around the trap. This constraint is given by constraining the trapezoid angle α_i and the length of the groove walls l_i, i.e., $C_3 = \{-\alpha_i \le -5°, -\tilde{l}_i \le -\tilde{r}_i\}$.
- Constraint C_4 is to avoid channel clogging, which is formulated by constraining the channel width g_i and the distance v_i between a trap and a microsphere filled in a consecutive row to be larger than the microsphere's diameter, i.e., $C_4 = \{\tilde{g}_i \le 4\tilde{r}_i - 2/h_i, -\tilde{g}_i \le -2\tilde{r}_i - 2/h_i, -\tilde{v}_i \le -2\tilde{r}_i - 2/h_i\}$.
- Constraint C_5 is to ensure a feasible fabrication, i.e., the possible aspect ratios (the ratio of transverse dimensions to height, for example, $\tilde{t}_i = t_i/h_i$) of the geometric parameters should be limited in the range of [0.4, 2.5]. This constraint is given by $C_5 = \{\tilde{l}_i, \tilde{g}_i, \tilde{b}_i, \tilde{u}_i, \tilde{t}_i \le 2.5, -\tilde{l}_i, -\tilde{g}_i, -\tilde{b}_i, -\tilde{u}_i, -\tilde{t}_i \le 0.4\}$.

- Constraint C_6 is to satisfy the optimal distance $d_{i,\text{opt}}$ between microspheres obtained in the statistical design to minimize image analysis error,[18,19] i.e., the distance d_i between the centers of two immobilized microspheres should be greater than $d_{i,\text{opt}}$, $C_6 = \{-\widetilde{d_\iota} \le -d_{i,\text{opt}}/h_i\}$.

In our design strategy, we expect the large microspheres to be immobilized by the large traps, while the small microspheres flow through the channels or the openings of the large traps, and then are immobilized by the small traps. This requirement adds one constraint (C_7) in the optimization of the large traps' geometric parameters, i.e., the bottom width of the large trap opening b_1 should be larger than the diameter of the small microsphere ($\widetilde{b_1} > 2\widetilde{r_2}$). To avoid the cases when fabrication variations hinder the values of the parameter to satisfy the constraint, we use a 2 μm safety margin[20] in the limit (note that this safety margin is also used in constraints C_2 and C_4). Therefore, $C_7 = \{-\widetilde{b_1} \le -2\widetilde{r_2} - 2/h_1\}$.

Furthermore, though the concentrations of the microspheres are carefully controlled to ensure the microspheres of each size will be fully immobilized at their corresponding region, there might be excess large microspheres flowing into the small trap region in the worst case. To avoid channel clogging by the large microspheres, we add one constraint C_8 on the channel width g_2 and the distance v_2 with respect to the large microspheres' radius r_1, i.e., $C_8 = \{\widetilde{g_2} \le 4\widetilde{r_1} - 2/h_2,\ -\widetilde{g_2} \le -2\widetilde{r_1} - 2/h_2,\ -\widetilde{v_2} \le -2\widetilde{r_1} - 2/h_2\}$.

To summarize, the optimization problem for the proposed microfluidic microsphere-trap arrays for simultaneous detection of two types of targets is

$$\rho_{i,\text{opt}} = 1/S_{i,\text{opt}}, \text{ with } S_{i,\text{opt}} = h_i^2 \cdot \min_{\boldsymbol{\delta}_i}\left(\widetilde{g_\iota} + \widetilde{l_\iota}\right) \cdot \left(\widetilde{u_\iota} + 2\widetilde{t_\iota} + \widetilde{g_\iota}\right), \quad i = 1 \text{ and } i = 2, \tag{2}$$

where $\boldsymbol{\delta}_1 \in \{C_1 \cap C_2 \cap C_3 \cap C_4 \cap C_5 \cap C_6 \cap C_7\}$, providing the feasible parameter spaces for the large microspheres and traps; and $\boldsymbol{\delta}_2 \in \{C_1 \cap C_2 \cap C_3 \cap C_4 \cap C_5 \cap C_6 \cap C_8\}$, providing the feasible parameter spaces for the small microspheres and traps.

Now we discuss the selection of some geometric parameters to demonstrate our design in the fluid dynamics simulations and experiments in the next two sections. For simplicity, we assume the values of the microspheres' radius r_1 and r_2 are known. We also keep the values of the channel heights h_1 and h_2 fixed. We further denote the remaining parameters in $\boldsymbol{\delta}_1$ and $\boldsymbol{\delta}_2$ as the optimization parameters. To tolerate manufacture variations on the sizes of the large and the small microspheres, the values of their radius (r_1 and r_2) should be selected distinct enough with each other. For example, in the fluid dynamics simulations in next section, we select $r_1 = 7.5$ μm and $r_2 = 5$ μm, respectively. To simplify the chip fabrication, we assign the same value to h_1 and h_2 ($h_1 = h_2 = h$), which act as normalizing factors in the optimization but do not affect the packing densities of the trap arrays. As discussed in Ref. 17, the channel height should be larger than one microsphere's diameter to avoid the microsphere flowing out of the channel, while it should be shallow enough to avoid one microsphere flowing on top of another microsphere so that the two arrive at the trap simultaneously to cause multiple trapping. Here, based on experimental testing, for $r_1 = 7.5$ μm and $r_2 = 5$ μm, we choose $h = 2.2r_1 = 3.3r_2 = 16.5$ μm. Furthermore, the minimal distances $d_{1,\text{opt}}$ and $d_{2,\text{opt}}$ to minimize the imaging errors for microspheres of radius $r_1$and r_2 are 30 μm and 20 μm, respectively.[20]

To solve the optimization problems for the large trap arrays and the small trap arrays, we use the grid-search method[21] on the feasible parameter spaces defined by $\boldsymbol{\delta}_1$ and $\boldsymbol{\delta}_2$. The optimal values of geometric parameters are summarized in Table 1 (the parameters d_1, d_2, v_1, and v_2 are not listed as they are functions of the other parameters).

Table 1. Fixed and optimization geometric parameters for the microfluidic microsphere-trap arrays for simultaneous detection of two types of targets.

Fixed values (μm)	r_1 7.5	r_2 5	h_1 16.5	h_2 16.5	
Optimized values for the large trap arrays (μm)	$l_{1,\text{opt}}$ 7.5	$u_{1,\text{opt}}$ 15.18	$b_{1,\text{opt}}$ 12	$t_{1,\text{opt}}$ 6.6	$g_{1,\text{opt}}$ 23.28
Optimized values for the small trap arrays (μm)	$l_{2,\text{opt}}$ 6.6	$u_{2,\text{opt}}$ 9.9	$b_{2,\text{opt}}$ 7.59	$t_{2,\text{opt}}$ 6.6	$g_{2,\text{opt}}$ 23.28

3. FINITE ELEMENT FLUIDIC DYNAMICS SIMULATIONS

To validate the applicability of the proposed design strategy, we use COMSOL Multiphysics 3.5[22] to perform finite element fluidic dynamics simulations of the transient motions of one large microsphere and one small microsphere flowing in the chip.

3.1 Simulation set-up

Given the high computational demand in three dimensional (3D) fluidic dynamics simulations, we perform two dimensional (2D) simulations. We note that the simulation domain (see Figs. 2 and 3) is the same as the layout in the schematic Fig. 1, and we precisely consider the geometric parameters of the microspheres and the traps as presented in Table 1. To compute the motions of the microspheres, the traps, and the fluid as well as for the hydrodynamic interactions among them, we employ three models (laminar flow model, solid mechanics model, and moving mesh model) given as follows.

Laminar flow model: The fluid flow in the microfluidic channels is assumed to be laminar flow. It is described by the incompressible Navier-Stokes equations[23] for the velocity field $\boldsymbol{u}_\mathrm{f} = (u_\mathrm{f}, v_\mathrm{f})$, and the pressure p_f, in the spatial (deformed) moving coordinate system:

$$\rho_\mathrm{f}\frac{\partial^2 \boldsymbol{u}_\mathrm{f}}{\partial^2 t} + \rho_\mathrm{f}(\boldsymbol{u}_\mathrm{f}\cdot\nabla)\boldsymbol{u}_\mathrm{f} = \nabla\cdot[-p_\mathrm{f}\boldsymbol{I} + \mu_\mathrm{f}(\nabla\boldsymbol{u}_\mathrm{f} + (\nabla\boldsymbol{u}_\mathrm{f})^T)] + \boldsymbol{F}_\mathrm{f}, \tag{3}$$

$$\rho_\mathrm{f}\nabla\cdot\boldsymbol{u}_\mathrm{f} = 0. \tag{4}$$

where, ρ_f denotes the fluid density (here, it is the water density of 1,000 kg/m^3), $\boldsymbol{u}_\mathrm{f}$ denotes the fluid velocity (m/s), t denotes the time (s), p_f denotes the pressure (Pa), $\boldsymbol{I}$ denotes the unit diagonal matrix, μ_f denotes the water dynamic viscosity (0.001 Pa·s), and $\boldsymbol{F}_\mathrm{f}$ is the volume force affecting the fluid (N/m^3).

We set the initial velocity field and pressure of the fluid in the simulation domain as $\boldsymbol{u}_\mathrm{f} = \boldsymbol{0}$ μm/s and $p_\mathrm{f} = 0$ Pa, respectively. At the inlet, the flow has fully developed laminar characteristics with a parabolic velocity profile and with centerline velocity along the flow direction as 15 μm/s. At the outlet, the boundary condition is $p_\mathrm{f} = 0$ Pa with no viscous stress. On the solid (non-deforming) walls such as the fixed traps and the simulation domain boundaries, we impose no-slip boundary condition to the fluid as $\boldsymbol{u}_\mathrm{f} = \boldsymbol{0}$ μm/s. On the deforming interface, i.e., the moving microspheres, we impose sliding-wall boundary condition to the fluid with velocity of the tangentially moving wall as 0 μm/s.

Solid mechanics model: The motion of the microspheres obeys Newton's laws of motion to a deformable solid[24]:

$$\rho_\mathrm{m}\frac{\partial^2 \boldsymbol{u}_\mathrm{m}}{\partial^2 t} - \nabla\cdot\boldsymbol{\sigma}_\mathrm{m} = \boldsymbol{F}_\mathrm{m} v_\mathrm{m}, \tag{5}$$

where, ρ_m denotes the microspheres' density (here, it is 1,062 kg/m^3 for the polystyrene microspheres), $\boldsymbol{u}_\mathrm{m} = (u_\mathrm{m}, v_\mathrm{m})$ denotes the microspheres' displacement field (m), $\boldsymbol{\sigma}_\mathrm{m}$ denotes the stress distribution within the microsphere, $\boldsymbol{F}_\mathrm{m} = (F_\mathrm{x,m}, F_\mathrm{y,m})$ denotes the boundary load (force) of the fluid on the surfaces of the microsphere, which is defined as force per unit area (N/m^2), and v_m denotes the microspheres' velocity.

We set the initial displacement field and the structural velocity field of the microspheres as $\boldsymbol{u}_\mathrm{m} = \boldsymbol{0}$ m and $\frac{\partial \boldsymbol{u}_\mathrm{m}}{\partial t} = \boldsymbol{0}$ m/s. We apply the linear elastic material model to the microspheres to allow for deformations, with the Young's modulus and Poisson's ratio of the microspheres set as 3.0 GPa and 0.33, respectively. The microspheres experience boundary load as described above.

Similar to the motion equation (Eqn. (5)) of the microspheres, the traps obey the following equation:

$$\rho_\mathrm{t}\frac{\partial^2 \boldsymbol{u}_\mathrm{t}}{\partial^2 t} - \nabla\cdot\boldsymbol{\sigma}_\mathrm{t} = \boldsymbol{F}_\mathrm{t} v_\mathrm{t}, \tag{6}$$

where, ρ_t denotes the traps' density (here, it is 965 kg/m^3 for the PDMS traps), $\boldsymbol{u}_\mathrm{t} = (u_\mathrm{t}, v_\mathrm{t})$ denotes the traps' displacement field (m), σ_t denotes the stress distribution within the trap, $F_\mathrm{t} = (F_\mathrm{x,t}, F_\mathrm{y,t})$ denotes the boundary load, and v_t denotes the microspheres' velocity.

Likewise, we set the initial displacement field and the structural velocity field of the traps as $\boldsymbol{u}_{\mathrm{t}} = \mathbf{0}$ m and $\frac{\partial \boldsymbol{u}_{\mathrm{t}}}{\partial t} = \mathbf{0}$ m/s. We apply the linear elastic material model to the traps, with the Young's modulus and Poisson's ratio of the traps set as 5.0 kPa and 0.33, respectively. We further set fixed constraint on the boundaries of the traps to ensure they are fixed in the fluid flow.

Moving mesh model: We create the predefined meshes of the simulation domain by the free triangular mesh method, with maximum element size as 2.24 μm, minimum element size as 0.32 μm, and resolution of curvature as 0.25. We further activate the calibration for fluid dynamics for mesh generation, to apply denser meshes in the fluid-solid interface region and looser meshes in the bulk fluid region. Then, we apply a freely moving deformed mesh to solve the Navier-Stokes equations and the Newton's laws of motion equations. The moving mesh constitutes the fluid domain and the solid domain (the microspheres and the traps), which enables adaptive modeling of the objects' transient motions and transfers the hydrodynamic interactions among them. We set the prescribed mesh displacements for the fixed trap and simulation domain boundaries as $\mathbf{0}$ m and for the microspheres as $\boldsymbol{u}_{\mathrm{m}}$ m. We also set the fluid domain as free deformation with initial mesh displacement as $\mathbf{0}$ m. To compute the deformation of the moving mesh relative to the initial shape of the domain, we use Winslow smoothing[25] with automatic re-meshing activated.

We perform the simulation by the time dependent solver in COMSOL. The dependent variables to compute are the velocity and the pressure of the fluid flow ($\boldsymbol{u}_{\mathrm{f}}$ and p_{f}); the displacements of the microspheres ($\boldsymbol{u}_{\mathrm{m}}$) and the traps ($\boldsymbol{u}_{\mathrm{t}}$); the boundary load on the microspheres ($\boldsymbol{F}_{\mathrm{m}}$); as well as the moving mesh frame coordinates. The computation of the dependent variables is given by two steps. At step 1, we solve for $\boldsymbol{u}_{\mathrm{f}}$ and p_{f} using Eqns. (3) and (4) with the defined initial and boundary conditions for the fluid. At step 2, we solve for $\boldsymbol{u}_{\mathrm{m}}$, $\boldsymbol{u}_{\mathrm{t}}$, and $\boldsymbol{F}_{\mathrm{m}}$ using Eqns. (5) and (6) and the solutions of $\boldsymbol{u}_{\mathrm{f}}$ and p_{f} computed at step 1, subject to the corresponding initial and boundary conditions. We solve these two steps iteratively until the end of the computation.

3.2 Simulation results

Recall that the microspheres of different sizes are loaded simultaneously to simplify operation; therefore we perform our simulations for two possible scenarios. In *Scenario 1*, we simulate one small microsphere flowing into the proposed trap arrays first, followed by one large microsphere. In *Scenario 2*, we simulate one large microsphere flowing into the arrays, followed by one small microsphere. Figs. 2 (*Scenario 1*) and 3 (*Scenario 2*) present the positions of the microspheres, as well as the fluid velocity surface plot and streamline plot, at several time points. Fig. 2 shows that the small microsphere flows through the large trap array region and is immobilized by one of its corresponding small trap. The subsequent large microsphere is immobilized by one of its corresponding large trap. Fig. 3 demonstrates that the large microsphere is immobilized by one of its corresponding large trap. The subsequent small microsphere bypasses the trap filled by the large microsphere, flows through the large trap array region, and finally is immobilized by one of its corresponding small trap. These finite element simulation results verify the applicability of the device design strategy for simultaneous detection of two types of targets.

4. PRELIMINARY EXPERIMENTAL RESULTS

In this section, we perform preliminary microsphere-trapping experiments using one microsphere size of radius 7.5 μm and show the designed trap geometry can successfully trap these microspheres with few errors and high efficiency. The fabrication and operation of these devices, as well as the experimental results are given below. To experimentally evaluate the performance of the proposed device for simultaneous detection of two types of targets, in the near future we will fabricate the devices with the optimized geometric parameters in Table 1.

4.1 Device fabrication and operation

The microsphere-trap array chip was connected by an inlet and an outlet. The optimized chip has a width of 1,000 μm and a length of 1,000 μm. The device, made of PDMS, was fabricated by using soft lithography techniques.[15] We first fabricated a master SU8 mold on a 3" silicon wafer using conventional photolithography. Then PDMS prepolymer (RTV615) was mixed at 1:10 A:B ratio and poured onto the mold and degassed in a vacuum chamber. The prepolymer was cured in an 80°C oven for 30 minutes. Then we peeled the partially cured PDMS off from the mold, and punched liquid inlet and outlet ports through the whole layer using a 0.75 mm diameter biopsy punch. Finally the PDMS layer ith fluidic pattern was permanently bonded to a standard glass slide by oxygen or air plasma treatment. The master molds could be reused many times.

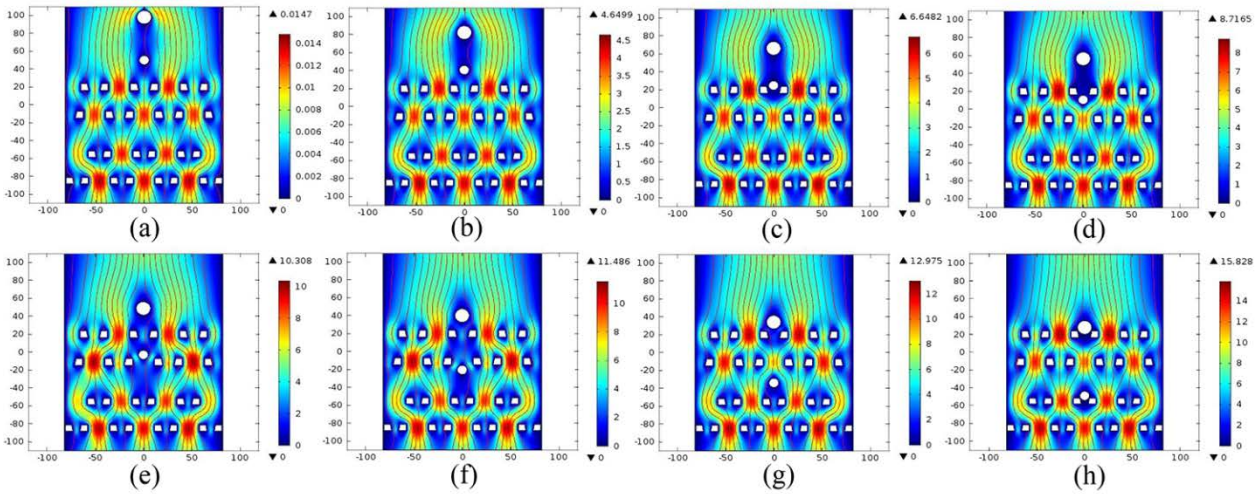

Fig. 2. Finite element fluid dynamics simulation of one small microsphere flowing in the proposed trap arrays, followed by one large microsphere (*Scenario 1*). The surface plot shows the fluid velocity magnitude (μm/s) and the streamline presents the spatial fluid velocity field. The small microsphere flows through the large trap array region and is immobilized by one of its corresponding small trap. The subsequent large microsphere is immobilized by one of its corresponding large trap.

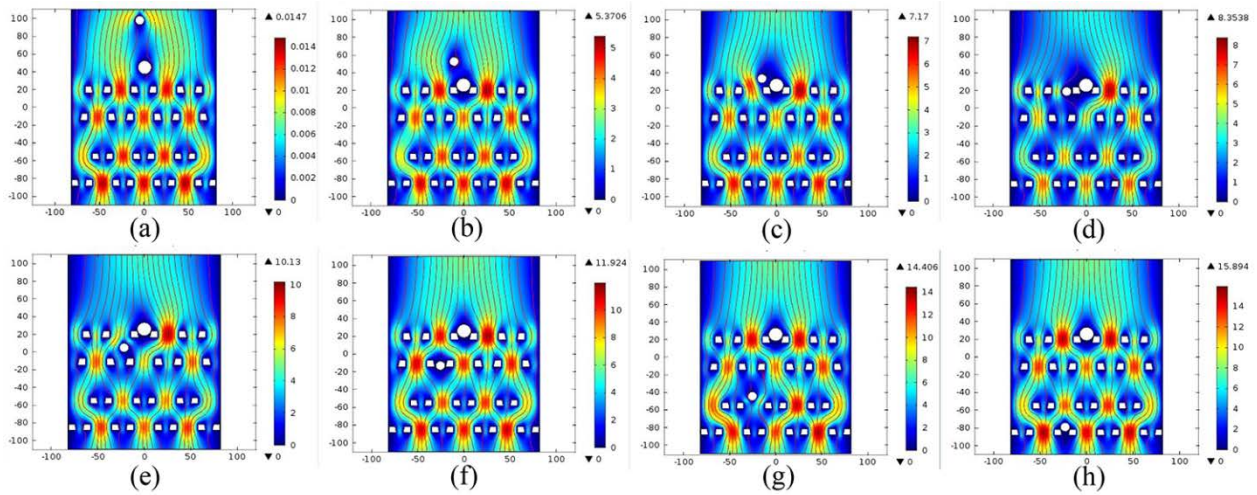

Fig. 3. Finite element fluid dynamics simulation of one large microsphere flowing in the proposed trap arrays, followed by one small microsphere (*Scenario 2*). The surface plot shows the fluid velocity magnitude (μm/s) and the streamline presents the spatial fluid velocity field. The large microsphere is immobilized by one of its corresponding large trap. The subsequent small microsphere bypasses the trap filled by the large microsphere, flows through the large trap array region, and finally is immobilized by one of its corresponding small trap.

The PDMS microfluidic trapping device was mounted on an inverted fluorescent microscope (Olympus IX71equipped with an EMCCD camera (Andor iXon+). A solution of 7.5 μm radius polystyrene microspheres (Bangs Lab, Fishers, IN) was prepared in 1X PBS buffer with 0.05% Tween-20 (Sigma Aldrich) at a concentration of 10^5/mL. The microsphere solution was loaded into a 22 gauge Tygon tubing (Cole Parmer). One end of the tubing was connected to the device input port via a stainless steel tube and the other end was connected to a compressed N_2 pressure source controlled by a pressure regulator with a resolution of 0.4 psi. The microsphere solution was pushed into the device by applying 1 psi pressure to the Tygon tubing. Snapshots and videos of the microsphere trapping process were captured by the EMCCD camera.

4.2 Results

Here we show the preliminary experimental results of a single microsphere trapping procedure in the device.

Fig. 4 presents the time sequence images of a single microsphere trapping process. It shows that our optimized trap geometry provides a low flow resistance path with a much smaller unit cell area compared with other designs.[26]

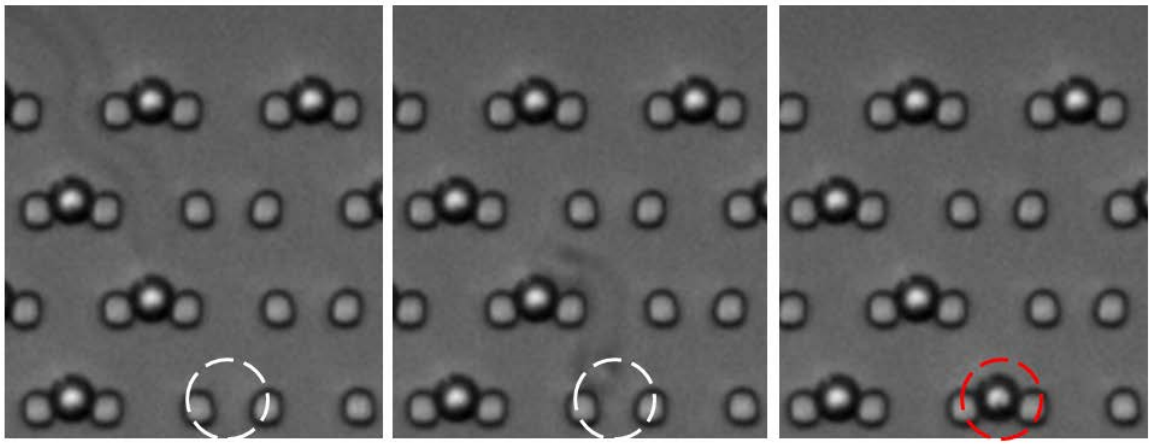

Fig. 4. Time lapse images of a 7.5 μm microsphere entering from top left and eventually captured by the trap indicated by the dashed circle.

Furthermore, it is important to have high trapping efficiency, i.e., a single microsphere in one trap (*single*), and to avoid fluidic errors such as multiple microspheres in one trap (*multiple*), empty traps (*empty*), and channel clogging (*clogged*) in order for the device to achieve its functions. Fig. 5 shows the trapping performance of the device. Explicitly, *single*, *multiple*, and *empty* are highlighted (there is no *clogged* in Fig. 5). The percentage of *empty* is close to 0% for the device, indicating that almost no traps remain empty at the end. As long as there are paths for the microspheres to reach the empty traps, these traps will be eventually filled. Nevertheless, filling the empty traps may in turn result in more microspheres trapped at a single trap or clog the channels. As observed from Fig. 5, our device has very few such errors. Furthermore, we almost never observe clogged channels when incoming microspheres are not clustered. In other words, in the device, most of the microspheres, if not immobilized in the empty traps, will pass by the channels directly. Therefore, in the device, *single* is dominant (99.29%) and the undesired *multiple* and *clogged* are negligible (0.38% and 0%, respectively). In summary, Fig. 5 confirms the outstanding performance of our device with highly reproducible experimental results and provides evidence for our proposed design for simultaneous detection of two types of targets.

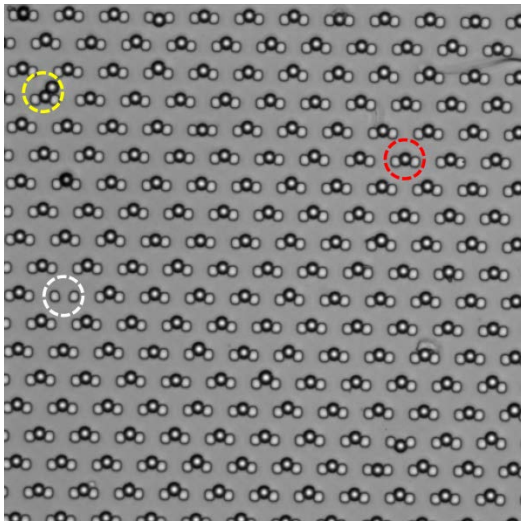

Fig. 5. Device performance. Highlighted areas: *single* (red dashed circle), *multiple* (yellow dashed circle), and *empty* (blue dashed circle). It can be seen that the optimized structure has few errors and most traps capture a single microsphere.

5. CONCLUSIONS

In this work, we proposed a microfluidic microsphere-trap array device for simultaneous, efficient, and accurate detection of multiple targets in a single-channel. We designed the trap array geometry by employing microspheres of difference sizes to capture different targets and extending our previous optimization framework.[17] We validated the design by finite element fluid dynamics simulations for microspheres of two different sizes. We also performed preliminary microsphere-trapping experiments on a fabricated device using microspheres of one size. The results validate that our device can achieve the position-encoding of the microspheres with high efficiency and few fluidic errors. Therefore, the proposed device is promising to achieve easy fabrication, convenient operation, and efficient detection of multiple targets.

In the near future, we will fabricate the proposed device for simultaneous detection of two types of targets and use microsphere-trapping experiments to investigate its performance. We will further validate its biological application potential by using it to detect epithelial growth factor receptor (EGFR) protein and mRNA, commonly over expressed in cancers of breast, lung, colon, etc. Overexpression of EGFR correlates with a poor prognosis and therefore carries significant predictive value in its quantification. We will estimate EGFR and EGFR mRNA expression levels and perform correlation analysis to accurately determine the significant values necessary for early detection of cancer.

ACKNOWLEDGEMENTS

This work was supported by National Science Foundation grant: CCF-0963742.

REFERENCES

[1] Xu, X., Sarder, P., Kotagiri, N., Achilefu, S., and Nehorai, A., "Performance analysis and design of position-encoded microsphere arrays using the Ziv-Zakai bound," IEEE Trans. on NanoBiosci, 12(1), 12 pages, doi: 10.1109/TNB.2012.2230116 (2013).

[2] Mathur, A., "Image analysis of ultra-high density, multiplexed, microsphere-based assays," Ph. D. thesis, Northwestern University, IL (2006).

[3] Epstein, J. R., Leung, A. P., Lee, K. H., and Walt, D. R., "High-density, microsphere-based fiber optic DNA microarrays," Biosens. Bioelectron., 18(5), 541-546 (2003).

[4] Schwenk, J. M., and Nilsson, P., "Antibody suspension bead arrays," Methods. Mol. Biol., 723, 29-36 (2011).

[5] Situma, C., Hashimoto, M., and Soper, S. A., "Merging microfluidics with microarray-based bioassays," Biomol. Eng., 23(5), 213-231 (2006).

[6] Liu, R.H., Dill. K., Fuji, H.S., McShea, A., "Integrated microfluidic biochips for DNA microarray analysis", Expert Rev. Mol. Diagn., 6(2), 253-61 (2006).

[7] Sarder, P., and Nehorai, A., "Estimating locations of quantum-dot–encoded microparticles from ultrahigh density 3D microarrays," IEEE Trans. on NanoBiosci., 7(4), 284-297 (2008).

[8] Rodiger, S., Schierack, P., Bohm, A., Nitschke, J., Berger, I., et al, "A highly versatile microscope imaging technology platform for the multiplex real-time detection of biomolecules and autoimmune antibodies," Adv. Biochem. Eng. Biotechnol., (2012).

[9] Rhee, W. J., and Bao, G., "Simultaneous detection of mRNA and protein stem cell markers in live cells," BMC Biotechnol., 9(30), 10 pages, (2009).

[10] Grover, W.H., Ivester, R.H.C., Jensen, E.C., and Mathies, R.A., "Development and multiplexed control of latching pneumatic valves using microfluidic logical structures," Lab Chip, 6(5), 623-631 (2006).

[11] Thorsen, T., Maerkl, S.J., and Quake, S.R., "Microfluidic large scale integration," Science, 298(5593), 580-584 (2002).

[12] Bohm, S., Burger, G. J., Korthorst, M. T., and Roseboom, F., "A micromachined silicon valve driven by a miniature bi-stable electro-magnetic actuator," Sens. Actuators, A, 80(1), 77-83 (2000).

[13] Capanu, M., Boyd, J. G., Hesketh, P. J., and Enikov, E., "Design, fabrication, and testing of a bistable electromagnetically actuated microvalve," J. Microelectromech. Syst., 9(2), 181-189 (2000).

[14] Pal, R., Yang, M., Johnson, B.N., Burke, D.T., and Burns, M.A., "Phase change microvalve for integrated devices," Anal. Chem., 76(13), 3740–3748 (2004).

[15] Li, Z., and Demetri, P., “Optofluidic distributed feedback dye lasers,” IEEE J. Sel. Top. Quant. Electron., 13(2), 185-193 (2007).
[16] Klemm, R., Hlawatsch, N., Hansen-Hagge, T. E., Becker, H., and Gartner, C., “Magnetic particle-based sample-prep and valveing in microfluidics,” Proc. SPIE 8251, 825108 (2012).
[17] Xu, X., Sarder, P., Li, Z., and Nehorai, A., “Optimization of microfluidic microsphere-trap arrays,” Biomicrofluidics 7, 014112 (2013).
[18] Sarder, P., and Nehorai, A., “Statistical design of position-encoded microsphere arrays,” IEEE Trans. NanoBiosci., 10(1), 16-29 (2011).
[19] Xu, X., Sarder, P., and Nehorai, A., "Statistical design of position-encoded microsphere arrays at low target concentrations," Proc. 45th Asilomar Conf. Signals, Syst. Comput., 1694-1698 (2011).
[20] Campbell, S. A., [The Science and Engineering of Microelectronic Fabrication], Oxford University Press, Oxford, Chapter 7 (2011).
[21] Kolda, T. G., Lewis, R. M., and Virginia, T., “Optimization by direct search: new perspectives on some classical and modern methods,” SIAM Rev., 45(3), 385-482 (2003).
[22] http://www.comsol.com/
[23] Bruus, H., [Theoretical microfluidics], Oxford University Press, Oxford, Chapter 2 (2008).
[24] Bower, A. F., [Applied mechanics of solids], CRC Press, Boca Raton, Chapter 2 (2009).
[25] Knupp, P. M., “Achieving finite element mesh quality via optimization of the Jacobian matrix norm and associated quantities. Part I-a framework for surface mesh optimization”, Int. J. Numer. Meth. Engng., 48, 401-420 (2000).
[26] Tan, W. H., and Takeuchi, S., “A trap-and-release integrated microfluidic system for dynamic microarray applications,” Proc. Natl. Acad. Sci. USA, 104(4), 1146-1151 (2007).
[27] Xu, X., Sarder, P., Li, Z., and Nehorai, A., “Optimization of microfluidic trap-based microsphere arrays,” Proc. SPIE 8615, 861533 (2013).